

Tracing the anomalous tqg and $tq\gamma$ flavor changing interactions at the FCC-he

Subhasish Behera* and Poulouse poulose†

Department of Physics, Indian Institute of Technology Guwahati, India.

We investigate the possible presence of *Flavor Changing Neutral Current (FCNC)* couplings of the top quark with gluon and photon through $e^-p \rightarrow e^-tj$ process. Focusing on disentangling the effects of different couplings that could be present, we exploit the presence of the scattered electron, the angular distribution of which is sensitive to the type of coupling involved. Further, we demonstrate the potential of electron beam polarisation in distinguishing the left-handed and right-handed couplings of both gluon and photon separately. Considering an e^-p collider of beam energies of $E_{e(p)} = 60$ (50000) GeV at 2 ab^{-1} integrated luminosity, couplings can be probed at the level of 10^{-2} with the corresponding branching fractions of $BR(t \rightarrow u\gamma) \leq 4 - 7 \times 10^{-6}$ and $BR(t \rightarrow c\gamma) \leq 1 - 2 \times 10^{-5}$, depending on if the coupling is right-handed or left-handed. The corresponding limits on the gluon couplings lead to $BR(t \rightarrow ug) \leq 1.7 \times 10^{-6}$ and $BR(t \rightarrow cg) \leq 3 - 4 \times 10^{-5}$.

CONTENTS

I. Introduction	1
II. Signal and Background	2
III. Event Generation and Analysis	3
IV. Top polarization Asymmetries	5
A. Disentangling different types of couplings	6
V. Summary and Conclusion	8
Acknowledgments	8
References	8

I. INTRODUCTION

Top quark has a special place in elementary particle dynamics. Discovered a little more than two decades ago, this heaviest elementary particle weighing about 185 times that of a proton is the only quark that decays weakly as a bare quark, the hadronization time being larger than its mean life time. This provides a unique window to explore the weak interactions of the quark sector in a direct way. Within the Standard Model (SM), quarks can have both charged current interactions with the mediation of charged gauge bosons, as well as neutral current interactions mediated by neutral gauge bosons. While by nature charged current interactions couple quarks of different flavours, Flavour Changing Neutral Current (FCNC) interactions are forbidden due to the GIM Mechanism [1]. Thus, while $t \rightarrow Wb$ decay is the most favoured channel, $t \rightarrow Zc$, γc , gc (where g represents a gluon) or those with c quark replaced by u quark are extremely rare. Absent at tree

level in the SM, higher order quantum corrections lead to $BR(t \rightarrow (Z/\gamma/g)c) \sim 10^{-14}$, which is suppressed by another two to three orders of magnitude in the case of u quarks [2]. The experimental measurements, on the other hand, are not yet capable of reaching out to such precision. Coming to the present constraints, the ATLAS collaboration of the LHC has performed a search for $t\gamma$ events with 81 fb^{-1} data at $\sqrt{s} = 13 \text{ TeV}$ [3]. Subsequently, they placed 95% C.L. bounds of $BR(t \rightarrow \gamma u) \leq 2.8 \times 10^{-5}$ for left-handed couplings and 6.2×10^{-5} for right-handed couplings; and $BR(t \rightarrow \gamma c) \leq 22 \times 10^{-5}$ and 88×10^{-5} for the left- and right-handed couplings, respectively. This is about an order of magnitude improvement on the bounds coming from a similar search by the CMS experiments [4]. Coming to tqg couplings, ATLAS collaboration searching for $qg \rightarrow t \rightarrow Wb$ process sets a limit on the branching fractions, $BR(t \rightarrow gu) \leq 4.5 \times 10^{-5}$ and $BR(t \rightarrow \gamma c) \leq 20 \times 10^{-5}$ using the 20.3 fb^{-1} data collected at the centre of mass energy of 8 TeV [5]. CMS search limits these coupling to 2.0×10^{-5} and 41×10^{-5} , respectively, from the 5 and 19.5 fb^{-1} data collected at $\sqrt{s} = 7$ and 8 TeV [6]. Anomalous top- Z FCNC couplings are bound by the ATLAS search for rare decays of the top quark in $t\bar{t}$ events at $\sqrt{s} = 13 \text{ TeV}$ with a data set of 36.1 fb^{-1} , setting a limit of $BR(t \rightarrow Zu) \leq 1.7 \times 10^{-4}$ and $BR(t \rightarrow Zc) \leq 2.4 \times 10^{-4}$ [7, 8]. Top-Higgs anomalous FCNC couplings are limited by the CMS search with $pp \rightarrow tH$ at centre of mass energy of 13 TeV with a data set of 35.9 fb^{-1} , bounding $BR(t \rightarrow Hq) \leq 0.47\%$, for both $q = u, c$ [9]. The ATLAS bounds on tqH FCNC from tH production at 13 TeV LHC with a data of 36.7 fb^{-1} is $BR(t \rightarrow Hu) \leq 2.4 \times 10^{-3}$ and $BR(t \rightarrow Hc) \leq 2.2 \times 10^{-3}$ [10]. At the same time, projected reach of these BR's at the high luminosity LHC with 3 ab^{-1} luminosity (HL-LHC) are $2.5 - 5.5 \times 10^{-5}$ [11], which is at the best an order of magnitude better than the current measurements. With the standard production of both the single top as well top-antitop pair in plenty, it is hard to probe anomalous top quark couplings in production at the LHC. A phenomenological study for top-antitop quark production at FCC-hh with 100 TeV center of mass at \mathcal{L} of 10 ab^{-1} sets limit on

* subhasish@iitg.ac.in; Also at Department of Physics, Johannes Gutenberg University Mainz, Germany.

† poulose@iitg.ac.in

the BR($t \rightarrow Hc$) $\leq \mathcal{O}(10^{-3})\%$ [12]. On the other hand, triple top quark production at the high energy versions of proton-proton collisions (HE-LHC and FCC-hh) has been proposed to probe the presence of FCNC, as the standard production in this case is forbidden [13–15]. It may be noted that colliders with electron beam has multiple advantages in probing the top quark FCNC, as illustrated in Ref. [16–20]. In particular, in Ref. [17] we have pointed out the possibility of distinguishing different Lorentz structures of the coupling studying the angular distributions of scattered electron and the asymmetries associated with it. Studying the single top production at FCC-ee, Ref. [21] showed that the Ztq and γtq couplings can be probed with the corresponding BR to the level of $3 - 5 \times 10^{-5}$ at a center of mass energy of 350 GeV with moderate luminosity of 300 fb^{-1} .

In this report, we shall study the process $ep \rightarrow ejt$, with subsequent leptonic decay of the top quark. We shall show that this process is suitable to probe tqg coupling in an effective way along with the $tq\gamma$ coupling. We parametrise the FCNC interactions of the top quark through the effective Lagrangian [22],

$$\begin{aligned}
-\mathcal{L}_{\text{fcnc}} = & g_s \bar{q} \lambda^a \frac{i\sigma^{\mu\nu} q_\nu}{\Lambda} (\kappa_{gqt}^L P_L + \kappa_{gqt}^R P_R) t G_\mu^a \\
& + e \bar{q} \frac{i\sigma^{\mu\nu} q_\nu}{\Lambda} (\kappa_{\gamma qt}^L P_L + \kappa_{\gamma qt}^R P_R) t A_\mu \\
& + \frac{g}{2c_W} \bar{q} \gamma^\mu (X_{zqt}^L P_L + X_{zqt}^R P_R) t Z_\mu \\
& + \frac{g}{2c_W} \bar{q} \frac{i\sigma^{\mu\nu} q_\nu}{\Lambda} (\kappa_{zqt}^L P_L + \kappa_{zqt}^R P_R) t Z_\mu + \text{H.c.}
\end{aligned} \tag{1}$$

where $q_\nu = p_t - p_q$, is the momentum transfer between the quarks in the process, and Λ is the cut-off scale. The vector couplings are denoted by $X_{zqt}^{L,R}$ for Z -boson and the tensor couplings by $\kappa_{gqt}^{L,R}$, $\kappa_{\gamma qt}^{L,R}$ and $\kappa_{zqt}^{L,R}$ for gluon, photon and Z -boson, respectively. The Feynman diagrams corresponding to $ep \rightarrow etj$ in the presence of these anomalous couplings are illustrated in Fig. 1. The scattered electron, posing like an innocent spectator turns out to be a valuable informer capable of providing clear indication of the Lorentz structure of the $tqZ(\gamma)$ couplings. This possibility alone is a marked advantage of the ep collider against the pp colliders. Demonstrating this, we shall study the angular asymmetry of the scattered electron as a useful discriminator between the gluon and photon couplings.

We shall organize this report as follows. In section II we discuss the signal and background process in details with cross section for different polarization of initial electron beam. In section III we discuss the event generation and analysis. In section IV we discuss various asymmetries and explore the possibility of discriminating different couplings. In section V we conclude the discussion.

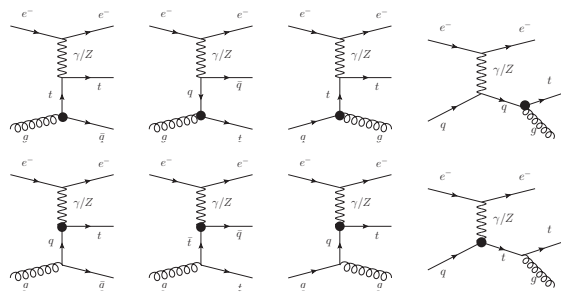


FIG. 1. Signal processes $pe^- \rightarrow e^- tj$. The final state has 32 diagrams at this collider.

II. SIGNAL AND BACKGROUND

The LHeC with proton beam energy of 7 TeV does not yield sufficient cross section, and therefore, we turn to the proposed FCC-he with possible proton beam energy of 50 TeV. The electron beam energy is set to 60 GeV in our analysis, which could be enhanced to 120 GeV with moderate increase in the cross section. At parton level the signal final state consists of $e^- b \ell \nu j$, where $\ell = e, \mu$. This final state does not arise in the SM for hard scattering process in ep collision. However, the SM processes with final states (i) $e^- jj\ell\nu$, (ii) $e^- bjj\ell\nu$, (iii) $bjjj\nu$, (iv) $bjj\nu$ and (v) $e^- jj\ell\nu$ could potentially mimic the signal after showering and hadronization. In table I, we have listed the cross section of the signal process for the production of top quark or anti-top quark with their subsequent leptonic (e^\pm, μ^\pm) decay, represented by σ_t and $\sigma_{\bar{t}}$, respectively, for different beam polarisations. The values quoted are for the u quark coupling with the top quark, which are slightly reduced when c quark is considered (owing to the smaller pdf) as listed in table II. We have considered one coupling to be present at a time setting its value to be unity, while setting all others to zero. Noticing that the cross section scales like the square of the coupling, one can obtain this for any value of the coupling in a straight forward way. If multiple couplings are considered, then there would be interference terms between those couplings in some scenarios.

In all cases of u -quark coupling, the top quark production cross section is about two times larger than that of the top antiquark production. This is mainly due to the difference in the *parton distribution function* (pdf) of the anti quark in proton compared to that of the quark. On the other hand, the c -quark couplings lead to more or less the same cross section for both top quark and top antiquark. This is also similar to the case of top antiquark cross section in the case of u -quark couplings, indicating the role of quark (or antiquark) pdf's play in the cross section. The electron beam polarisation is another influencing factor at this collider. The polarisation of the electron beam influence the reactions differently depending on the type of anomalous couplings. We shall exploit this fact to distinguish the couplings. In this study we

Coupling	κ_{gut}^L	κ_{gut}^R	$\kappa_{\gamma ut}^L$	$\kappa_{\gamma ut}^R$	X_{zut}^L	X_{zut}^R	κ_{zut}^L	κ_{zut}^R
unpolarized								
σ_t (fb)	526	557	1601	1602	263	251	310	337
$\sigma_{\bar{t}}$ (fb)	259	265	835	832	141	148	123	106
$P_{e^-} = -0.8$								
σ_t (fb)	546	696	1238	1968	332	274	320	441
$\sigma_{\bar{t}}$ (fb)	289	295	1102	564	154	187	174	96
$P_{e^-} = +0.8$								
σ_t (fb)	515	414	1965	1238	196	230	300	234
$\sigma_{\bar{t}}$ (fb)	231	235	565	1102	129	110	72	117

TABLE I. The partonic cross section of the signal process : $pe^- \rightarrow e^- tj, (t \rightarrow Wb, W \rightarrow l\nu_l)$ for different Vtu FCNC couplings. The value of the anomalous couplings are set to unity, and beam energies of $E_{e(p)} = 60$ (50000) GeV are considered.

shall focus on the tqg and $tq\gamma$ couplings, which spare better compared to the tqZ couplings.

Coupling	κ_{gct}^L	κ_{gct}^R	$\kappa_{\gamma ct}^L$	$\kappa_{\gamma ct}^R$	X_{zct}^L	X_{zct}^R	κ_{zct}^L	κ_{zct}^R
unpolarized								
σ_t (fb)	249	273	713	708	124	118	82	97
$\sigma_{\bar{t}}$ (fb)	245	249	710	707	119	124	97	81
$P_{e^-} = -0.8$								
σ_t (fb)	222	359	467	951	155	129	70	139
$\sigma_{\bar{t}}$ (fb)	271	277	954	465	130	155	139	70
$P_{e^-} = +0.8$								
σ_t (fb)	276	187	959	465	93	107	93	54
$\sigma_{\bar{t}}$ (fb)	218	221	466	949	107	92	54	93

TABLE II. The partonic cross section of the signal process : $pe^- \rightarrow e^- tj, (t \rightarrow Wb, W \rightarrow l\nu_l)$ for different Vtc FCNC couplings. The value of the anomalous couplings are set to unity, and beam energies of $E_{e(p)} = 60$ (50000) GeV are considered.

Coming to the background, we present the cross sections of listed potential processes in table III. Notice that choosing right-handed electron beam polarisation can reduce the backgrounds by a factor of 2 to 5, depending on the background process.

Process	σ (fb)		
	unpol	$P_e = -0.8$	$P_e = +0.8$
$e^- jj\ell^+\nu_l$	138	203	73
$e^- bj\ell^+\nu_l$	6	8	3
$bjjj\nu_\ell$	44	79	9
$bjj\nu_\ell$	144	260	29
$e^- jj\ell^-\nu_\ell$	153	240	69

TABLE III. The partonic cross section of the background processes (for both t and \bar{t} in the signal process) at different beam polarizations, with beam energies of $E_{e(p)} = 60$ (50000) GeV. Both e and μ are included in ℓ .

III. EVENT GENERATION AND ANALYSIS

We use the FeynRules implementation of the effective Lagrangian considered in eq. (1) in addition to the SM Lagrangian. For the event generation of both signal and background we use MADGRAPH5 [23], with a customised Pythia-PSG [24] performing the hadronization and showering. CTEQ6L1 pdf is used setting the factorization and renormalization scales to m_t . Generation level event selection of transverse momentum $p_T > 10$ GeV and pseudo rapidity $|\eta| < 5$ are imposed on all jets and leptons. The events thus generated are passed through FastJet [25] to form the jets, where we used the anti- k_T algorithm with cone size of $R = 0.4$. The detector is emulated through Delphes [26] with detector code tuned to take into account the asymmetric nature of the collider along with the very high energy proton beam resulting in highly boosted final state products. The events thus obtained after passing through Delphes are further analyzed using MadAnalysis5 [27] and ROOT [28]. The pre-selection of events is performed with the basic selection criteria

$$P_T^i > 10 \text{ GeV}, \quad |\eta_i| < 5, \quad \Delta R(i, j) \geq 0.4,$$

where $i, j \equiv$ electron, light-jet, or b-jet. Defined as usual $\Delta R = \sqrt{\Delta\eta^2 + \Delta\Phi^2}$, where η is the pseudo-rapidity and ϕ is the azimuthal angle. In the case of signal, we have considered the SM decay of top quark which further gives either a μ^+ or e^+ , and the top antiquark into μ^- final state. With the scattered electron always present, we have not considered the case of top antiquark decaying into electron, as the top quark reconstruction will be less efficient in this case. The above basic selection of events is followed by the signal specific event selection demanding

1. one isolated e^- ,
2. one isolated ℓ (either e^+ or μ^+ for top quark, and μ^- for top antiquark production)
3. one b -jet,
4. at least one light-jet.

This selection cuts down the signal by a factor of 2, whereas the background is reduced by a factor of 20. The cross sections before and after the selection are given in table IV for the case of unpolarised beam. Cases with the left- and right-beam polarisation are affected by this selection in a similar way. Only the $ejj\ell\nu$ background is significant after this selection. For further event selection to enhance the signal over background we studied the kinematic distributions. In fig. 2 some of the selected kinematic distributions are presented for the unpolarized electron beam, and considering the μ^+ decay channel of the top quark. All other cases of e^+ and μ^- in the final state, and with left- or right-polarised electron beams have similar distributions. We have analysed those cases separately, and the final results in each case shall be presented towards the end.

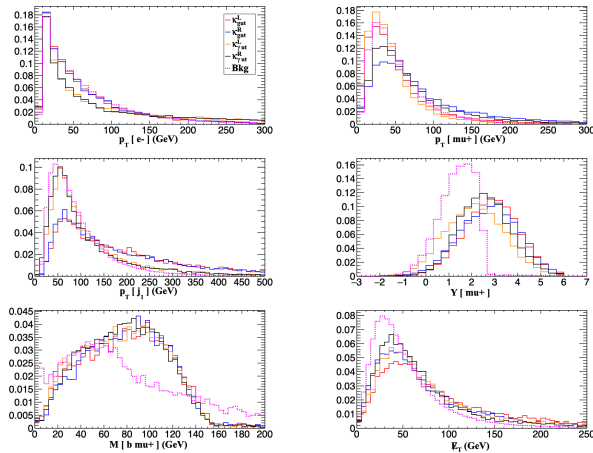


FIG. 2. Some of the kinematic distributions for the case of $e^-p \rightarrow e^-tj \rightarrow e^-j\mu^+\nu$ after the application of basic cuts and selecting out events with $N_{e^-} = N_{\mu^+} = N_b = 1$ and $N_j \geq 1$. The solid (dotted) line represents the signals (background) events. Different case of signal are as indicated.

Main distinguishing factor between the signal and the background is their prominent difference in the rapidity distribution of the decay lepton. We shall exploit this to employ suitable selections to enhance the signal significance. Thus we select a rapidity region of $Y_\ell > 2.6$ bringing down the signal by another factor of 2- 4, depending on the nature of the couplings considered and the polarization of the beam used (see table IV). The background, on the other hand, is considerably reduced with corresponding enhancement in the signal significance. The other two cases of beam polarisation with $P_e = \pm 0.8$ show very similar behaviour with the selection.

In the case of top quark production, the fiducial cross sections of the signal events range from 300 to 700 fb, considering individual decay channels of the top quark and for unit couplings with the energy scale set to mass of the top quark ($\Lambda = m_t$). For top anti-quark we consider only the μ^- channel, with the cross section after selection in the range of 50 to 150 fb. For more realistic coupling values of $\kappa^{L,R} = 1 - 2 \times 10^{-2}/m_t$, the cross section will be

Coupling	κ_{gut}^L	κ_{gut}^R	$\kappa_{\gamma ut}^L$	$\kappa_{\gamma ut}^R$	κ_{gct}^L	κ_{gct}^R	$\kappa_{\gamma ct}^L$	$\kappa_{\gamma ct}^R$	Bkg
$e^-p \rightarrow e^-tj \rightarrow e^-j\ell^+\nu$ (both e^+ and μ^+ included)									
Basic Cuts	1058.0	1113.2	3198.0	3190.0	498.5	546.2	1420.2	1420.0	485.0
$N_{e^-} = N_{e^+} = N_b = 1, N_j \geq 1$	515	550.0	1631.7	1623.2	245.9	271.5	728.1	737.0	8.5
$Y_{\mu^+} > 2.6$	290.1	287.6	530.3	715.8	105.4	82.8	155.9	219.0	0.023
$e^-p \rightarrow e^-tj \rightarrow e^-j\mu^-\nu$									
Basic Cuts	259.4	266.1	831.7	829.1	244.0	248.8	709.4	708.9	485.0
$N_{e^-} = N_{\mu^-} = N_b = 1, N_j \geq 1$	146.4	150.1	467.7	480.1	130.6	128.8	374.1	376.6	4.8
$Y_{\mu^-} > 2.6$	65.8	53.6	102.5	151.0	58.3	47.2	79.6	118.2	0.009

TABLE IV. Cross sections (σ fb) with unpolarised electron beam at different selections levels. The signal is considered with coupling values taken as unity, and the background is denoted as Bkg.

reduced by a factor corresponding to the square of the coupling. The best case scenario of ℓ^+ final state is listed in table V, taking the coupling to be $\frac{\kappa^2}{\Lambda^2} = \frac{2 \times 10^{-4}}{m_t^2}$, along with the signal sensitivity reachable at 2 ab^{-1} luminosity.

$\kappa^2 = \frac{2 \times 10^{-4}}{m_t^2}$	κ_{gut}^L	κ_{gut}^R	$\kappa_{\gamma ut}^L$	$\kappa_{\gamma ut}^R$	κ_{gct}^L	κ_{gct}^R	$\kappa_{\gamma ct}^L$	$\kappa_{\gamma ct}^R$
unpolarized beam. Background events, $N_B = 46$								
Signal, N_S	116	115	212	286	42	33	62	88
Significance	9.1	9.0	13.2	15.7	4.5	3.7	6.0	7.6
$P_e = -0.8$. Background events, $N_B = 34$								
Signal, N_S	128	135	197	324	52	70	74	157
Significance	10.1	10.4	13.0	17.1	5.6	6.9	7.1	11.3
$P_e = +0.8$. Background events, $N_B = 28$								
Signal, N_S	109	125	195	328	56	42	116	95
Significance	9.3	10.1	13.0	17.4	6.1	5.0	9.6	8.6

TABLE V. Signal significance with an assumed value of the coupling, $\frac{\kappa^2}{\Lambda^2} = \frac{2 \times 10^{-4}}{m_t^2}$ for the process $e^-p \rightarrow e^-tj \rightarrow e^-j\ell^+\nu$ (ℓ^+ includes both e^+ and μ^+). An integrated luminosity of 2 ab^{-1} is considered.

The significance is computed using the formula

$$\text{Significance} = \frac{N_S}{\sqrt{N_S + N_B}}. \quad (2)$$

The left polarised beam shows a marginally better significance as compare to other two samples. To obtain the reach of the coupling at a given confidence level, in fig. 3 we plot the significance against the number of signal events. Both the cases of $t \rightarrow b\ell^+\nu$ (solid curve) adding μ^+ and e^+ events, and $\bar{t} \rightarrow b\mu^-\bar{\nu}$ (dotted curve) are presented for three different electron beam polarisations considered, along with the black dashed line indicating the 95% C.L. value. The number of events required to have 95% C.L., for the three different cases of polarizations are given in table VI, along with the corresponding reach on the couplings, setting the cut-off $\Lambda = 1 \text{ TeV}$. The branching ratios of the corresponding rare channels

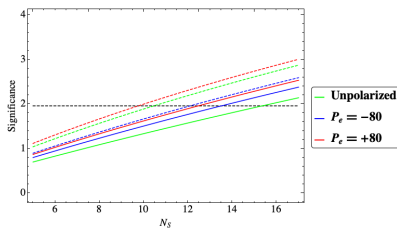


FIG. 3. Significance against the number of signal events required for specific number of background events as per Eq. 2. Number of background events corresponding to the cases of $e^-p \rightarrow e^-tj \rightarrow e^-j\ell^+\nu$ including both e^+ and μ^+ in the final state (solid lines), and that corresponding to the case of $e^-p \rightarrow e^-tj \rightarrow e^-j\mu^-\nu$ (dotted lines) considered for the three beam polarisations.

Beam polarization	Associated quark	Background events, N_B	Required signal, $N_S(2\sigma)$	Reach of couplings for 95% CL. (TeV^{-1})			
				κ_{Vqt}^L/Λ	κ_{Vqt}^R/Λ	$\kappa_{\gamma qt}^L/\Lambda$	$\kappa_{\gamma qt}^R/\Lambda$
Unpolarized	<i>up</i>	46	16	0.029	0.029	0.021	0.019
	<i>charm</i>			0.048	0.054	0.040	0.033
(-80%)	<i>up</i>	34	14	0.028	0.027	0.022	0.017
	<i>charm</i>			0.043	0.037	0.036	0.025
(+80%)	<i>up</i>	28	13	0.030	0.030	0.022	0.019
	<i>charm</i>			0.050	0.056	0.041	0.035

TABLE VI. Number of signal events required for 2σ significance (refer to fig. 3), and the 95% C.L. reach on the corresponding couplings for different beam polarizations in $e^-p \rightarrow e^-tj \rightarrow e^-j\ell^+\nu$ (with ℓ^+ including both e^+ and μ^+) at an integrated luminosity of 2 ab^{-1} .

in the best case scenario of -80% beam polarisation is comparable to, and in some cases marginally better than that achievable at the HL-LHC (notice that we consider smaller integrated luminosity than what is considered in the case of HL-LHC), as given in table VII. The cases of unpolarised beam and right-polarised beam have similar reach, with marginal differences. Judging from the num-

Coupling	BR $\times 10^5$			
	$t \rightarrow ug$	$t \rightarrow cg$	$t \rightarrow u\gamma$	$t \rightarrow c\gamma$
κ_{Vqt}^L/Λ	1.8	4.3	0.74	1.9
κ_{Vqt}^R/Λ	1.7	3.1	0.44	0.95

TABLE VII. 95% C.L. reach on the branching fractions of the rare decay, corresponding to the reach on the relevant coupling (as in table VI) in the best case of -80% beam polarisation with 2 ab^{-1} integrated luminosity.

bers in table IV the case of top antiquark is very similar to that of the c quark couplings in top production case. Thus, for the u quark coupling, top quark case has an edge over the top antiquark case, whereas for the c quark couplings, both give similar results. Besides considering separately, one may perform a combined analyses of all the cases, which may increase the sensitivity significantly. However, we do not attempt this in the present discus-

sion.

IV. TOP POLARIZATION ASYMMETRIES

In this section we discuss the formalism that could be employed to extract the polarization information of the top quark through suitably constructed observables. For details of the formalism one may consult Ref. [17] and references therein. The motivation for the spin analysis of top quark comes from the fact that the angular distributions of top quark decay products give access to the Lorentz structure of the production vertex through the information of top quark polarisation. To extract the information we proceed as follows.

In the Narrow Width Approximation (NWA), the invariant amplitude square of the full process ($eq \rightarrow etj \rightarrow ejb\ell\nu$) can be written as a product of the production and decay density matrices in the helicity basis of the top quark as

$$|\mathcal{M}|^2 = \frac{\pi\delta(p_t^2 - m_t^2)}{\Gamma_t m_t} \sum_{\lambda, \lambda'} \rho(\lambda, \lambda') \Gamma(\lambda, \lambda'), \quad (3)$$

where p_t is the momentum and Γ_t is the total width of the top quark, with the summation considered over the helicity indices of the top quark. The production and decay density matrices are given in terms of the corresponding amplitudes as $\rho(\lambda, \lambda') = \mathcal{M}_P(\lambda) \mathcal{M}_P^*(\lambda')$ and $\Gamma(\lambda, \lambda') = \mathcal{M}_\Gamma(\lambda) \mathcal{M}_\Gamma^*(\lambda')$, respectively. The top quark on-shell condition in the NWA allows one to write the differential cross section of the complete process as [29]

$$\frac{1}{\sigma_t} \frac{d\sigma_t}{d\Omega_t} = \frac{1}{4\pi} \sum_{\lambda, \lambda'} \sigma(\lambda, \lambda') \Gamma(\lambda, \lambda') \quad (4)$$

where we define the normalised production density matrix of the top quark,

$$\sigma(\lambda, \lambda') = \frac{1}{\sigma_{\text{prod}}} \int \rho(\lambda, \lambda') d\Omega_t, \quad (5)$$

with $d\Omega_t$ representing the differential solid angle of top quark produced and σ_{prod} denoting the total production cross section. For convenience, we define polarisation vector $\mathbf{P} = (P_x, P_y, P_z)$ so that

$$\begin{aligned} \sigma(+, +) &= \frac{1}{2}(1 + P_z), & \sigma(+, -) &= \frac{1}{2}(P_x + iP_y), \\ \sigma(-, -) &= \frac{1}{2}(1 - P_z), & \sigma(-, +) &= \frac{1}{2}(P_x - iP_y). \end{aligned} \quad (6)$$

The normalized decay density matrix elements for the process $t \rightarrow W^+b \rightarrow b\ell^+\nu_\ell$ may be written in terms of the polar (θ_ℓ) and azimuthal (ϕ_ℓ) angles of the secondary

lepton in the top rest frame as [29],

$$\begin{aligned}\Gamma(+, +) &= \frac{1}{2}(1 + \cos \theta_\ell), & \Gamma(+, -) &= \frac{1}{2} \sin \theta_\ell e^{i\phi_\ell}, \\ \Gamma(-, -) &= \frac{1}{2}(1 - \cos \theta_\ell), & \Gamma(-, +) &= \frac{1}{2} \sin \theta_\ell e^{-i\phi_\ell}.\end{aligned}\quad (7)$$

Here the polar angle is measured with respect to the top quark boost direction, and the top production plane is taken as the x - z plane. These choices of reference do not cost us generality of the analysis as shown in Ref. [30]. The differential cross section for the complete process in terms of the top quark polarisation vector and the polar and azimuthal angle of the secondary lepton in the rest frame of the top quark, can now be written as

$$\frac{1}{\sigma_t} \frac{d\sigma_t}{d\Omega_\ell} = \frac{1}{4\pi} \left(1 + P_z \cos \theta_\ell + P_x \sin \theta_\ell \cos \phi_\ell + P_y \sin \theta_\ell \sin \phi_\ell \right), \quad (8)$$

where Ω_ℓ is the solid angle of the secondary lepton. This enables one to define angular asymmetries of the secondary leptons, and connect those directly to the top quark polarisation. The following three asymmetries, two defined in terms of the azimuthal angle, and one in terms of the polar angle of the decay lepton, are used in the subsequent study.

$$\begin{aligned}A_x &\equiv \frac{1}{\sigma_{\text{tot}}} \left[\int_{-\frac{\pi}{2}}^{\frac{\pi}{2}} d\phi_\ell \frac{d\sigma}{d\phi_\ell} - \int_{\frac{\pi}{2}}^{\frac{3\pi}{2}} d\phi_\ell \frac{d\sigma}{d\phi_\ell} \right] = \frac{1}{2} P_x, \\ A_y &\equiv \frac{1}{\sigma_{\text{tot}}} \left[\int_0^\pi d\phi_\ell \frac{d\sigma}{d\phi_\ell} - \int_\pi^{2\pi} d\phi_\ell \frac{d\sigma}{d\phi_\ell} \right] = \frac{1}{2} P_y, \\ A_z &\equiv \frac{1}{\sigma_{\text{tot}}} \left[\int_0^1 dc_{\theta_\ell} \frac{d\sigma}{dc_{\theta_\ell}} - \int_{-1}^0 dc_{\theta_\ell} \frac{d\sigma}{dc_{\theta_\ell}} \right] = \frac{1}{2} P_z.\end{aligned}\quad (9)$$

Note that the angles in the above asymmetries are defined in the rest frame of the top quark, and thus require full reconstruction of the top quark momentum. In the present case this leads to the following relations between the components of the missing momentum (neutrino in this case) denoted by $p_{x\nu}$, $p_{y\nu}$, $p_{z\nu}$, and those of the visible final particles.

$$\begin{aligned}p_{x\nu} &= - \sum_{k=e,j,\ell,b} p_{xk}, & p_{y\nu} &= - \sum_{k=e,j,\ell,b} p_{yk}, \\ (p_{z\nu})_\pm &= \frac{1}{p_{T\ell}^2} \left[\beta p_{z\ell} \mp E_\ell \sqrt{\beta^2 - p_{T\nu}^2 p_{T\ell}^2} \right],\end{aligned}\quad (10)$$

where $\beta = \frac{m_W^2}{2} + p_{x\ell} p_{x\nu} + p_{y\ell} p_{y\nu}$ and $p_{T_i}^2 = p_{x_i}^2 + p_{y_i}^2$. Out of the above two solutions for $p_{z\nu}$, the one for which $|\sum_r p_r^2 - m_i^2|$ is minimum, where p_r is the four momentum of the corresponding particle, with $r = \ell, b, \nu$, will be considered as the correct choice for the z -component. The missing momentum thus obtained is used to reconstruct the top quark momentum.

In addition to the asymmetries related to secondary lepton, we may exploit the advantage of producing the

top quark in association with the electron in distinguishing the nature of the coupling. In fig. 4 we plot the angular distributions of the scattered electron in the lab frame of the collider. As seen, the polar angle of the electron is sensitive to whether gluon coupling (tgq) or photon coupling ($t\gamma q$) is considered. This is in a way intuitively clear, as the scattered electron interact with the quarks through photon or Z , and thus decoupled from the effects in the gluon interactions. On the contrary it is seen to be insensitive to the case of anti top quark production, indicating that the forward scattering of the electrons are dominated by the quark initiated processes. We define the forward-backward asymmetry,

$$A_{e^-}^{FB} = \frac{\sigma(\cos \theta_{e^-} > 0) - \sigma(\cos \theta_{e^-} < 0)}{\sigma(\cos \theta_{e^-} > 0) + \sigma(\cos \theta_{e^-} < 0)}, \quad (11)$$

where we denote the polar angle of the electron by θ_{e^-} . Numerical values of all the three asymmetries for differ-

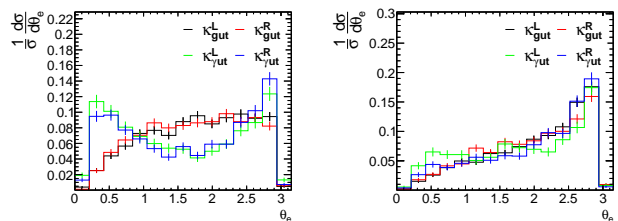


FIG. 4. Angular distribution of the scattered electron in the case of unpolarised beam normalised to unity. The left figure corresponds to the top quark production, while the right one corresponds to the top antiquark production.

ent couplings used are presented in table VIII in the case of top quark production with ℓ^+ in the final state, and in table IX in the case of top antiquark production with μ^- in the final state.

Coupling	No pol.			$P_{e^-} = -80\%$			$P_{e^-} = +80\%$		
	A_x	A_z	$A_{e^-}^{FB}$	A_x	A_z	$A_{e^-}^{FB}$	A_x	A_z	$A_{e^-}^{FB}$
κ_{gut}^L	-0.20	-	-0.22	-0.27	-	-0.28	-0.21	-	-0.20
κ_{gut}^R	0.14	0.40	-0.15	0.16	0.42	-0.23	0.11	0.41	-0.16
$\kappa_{\gamma ut}^L$	-0.33	-0.12	-	-0.31	-0.11	-	-0.30	-0.16	-
$\kappa_{\gamma ut}^R$	-	0.46	-	-	0.47	-	-	0.48	-

TABLE VIII. Top polarisation asymmetries and forward-backward asymmetry of the scattered electron with three different beam polarisations, considering presence of one coupling at a time in the process $e^- p \rightarrow e^- \bar{u} t$ with $t \rightarrow b \ell^+ \nu$.

A. Disentangling different types of couplings

We shall turn to the possibility to identify the type of coupling present by making use of a combination of

Coupling	No pol.			$P_{e^-} = -80\%$			$P_{e^-} = +80\%$		
	A_x	A_z	A_e^{FB}	A_x	A_z	A_e^{FB}	A_x	A_z	A_e^{FB}
κ_{gut}^L	-0.35	0.26	-0.48	-0.32	0.28	-0.48	-0.34	0.19	-0.46
κ_{gut}^R	-	0.33	-0.39	-	0.41	-0.47	-	0.32	-0.35
$\kappa_{\gamma ut}^L$	-0.44	-	-0.25	-0.43	-	-0.28	-0.45	-	-0.28
$\kappa_{\gamma ut}^R$	-0.11	0.54	-0.44	-0.14	0.56	-0.37	-	0.53	-0.39

TABLE IX. Top polarisation asymmetries and forward-backward asymmetry of the scattered electron with three different beam polarisations, considering presence of one coupling at a time in the process $e^- p \rightarrow e^- u \bar{t}$ with $\bar{t} \rightarrow \bar{b} \mu^- \bar{\nu}$.

observables discussed above. To start with we may notice that a comparison of event rates with different beam polarizations could be useful here. To illustrate this, we shall consider the fiducial cross sections after the event selection quoted in table V for top quark production and its leptonic decay. We shall first consider the u quark coupling, where going from unpolarised beam to -80% polarised beam, the cross section is increased by 10 - 18% for the case of gluon couplings and right-handed photon coupling. In the case of left-handed photon coupling, it has an increase, but less than 10%. Going from unpolarised to $+80\%$ polarised beams, only the right-handed photon coupling present an appreciable change of a increase by about 15%, with all other cases registering a less than 10% change. On the other hand, switching the polarisation from -80% to $+80\%$ leaves all cases within the 10%, except the left-handed gluon coupling, which shows a decrease of about 15%. Coming to the case of c quark coupling, the changes are more dramatic, indicating that the quark initiated processes are more sensitive to the electron beam polarisation. In this case, going from unpolarised beam to -80% beam polarisation shows an increase in all cases, with about 80% and 112% in the case of photon and gluon right-handed couplings, respectively. Moving from unpolarised to $+80\%$ polarised beam, on the other hand, while showing increase in all cases, the left-handed photon coupling poses a large difference of close to 90%, while the right-handed photon case registering only small change. Switching the polarisation from left- to right-handed shows considerable downward change in the case of right-handed couplings in both the cases, while the left-handed case is undemocratic with the photon case showing a large increase of about 57%, and the gluon case showing small decrease of about 7%. We summarise these qualitative features in the cartoon in table X.

The qualitative features of the behaviour of the top polarisation asymmetries (A_x , A_z) and electron forward-backward asymmetry (A_e^{FB}) are also useful discriminator of the type of coupling. In table XI we capture these features in the case of top quark production. First of all, the forward-backward asymmetry of the scattered electron is absent in the case of photon couplings. A_z asymmetry

(\dots : $< 10\%$ change), (\downarrow or \uparrow : $\sim 10\% - 50\%$), (\Downarrow or \Uparrow : $> 50\%$)

	unpol $\rightarrow -80\%$	unpol $\rightarrow +80\%$	$-80\% \rightarrow +80\%$
u quark couplings			
$\kappa_{\gamma ut}^L$	\dots	\dots	\dots
$\kappa_{\gamma ut}^R$	\uparrow	\uparrow	\dots
κ_{gut}^L	\uparrow	\dots	\downarrow
κ_{gut}^R	\uparrow	\dots	\dots
c quark couplings			
$\kappa_{\gamma ct}^L$	\uparrow	\Uparrow	\Uparrow
$\kappa_{\gamma ct}^R$	\Uparrow	\dots	\downarrow
κ_{gct}^L	\uparrow	\uparrow	\dots
κ_{gct}^R	\Uparrow	\uparrow	\downarrow

TABLE X. Demonstrating the power of beam polarization to disentangle the effects of different types of couplings. The up- or down-arrows indicate an increase or decrease in the number of events. For the number of events at 2 ab^{-1} luminosity, see table V.

is positive and large (close to 50%) in the case of right-handed couplings. Thus, presence of A_{FB}^e along with positive A_z will indicate the presence of κ_{gut}^R . If A_z is absent, on the other hand, the coupling responsible is κ_{gut}^L . If A_{FB}^e is absent and A_z is large and positive it indicates $\kappa_{\gamma ut}^R$, whereas negative A_z indicates the presence of $\kappa_{\gamma ut}^L$. Presence or absence of A_x along with its sign can be used as additional marker. These qualitative distinctions comparing the asymmetries are independent of the beam polarization. In the case of top antiquark, the

From top quark				From top antiquark			
A_x	A_z	A_e^{FB}	Coupling	A_x	A_z	A_e^{FB}	Coupling
-ve	\dots	-ve	κ_{gut}^L	-ve	+ve	-ve	κ_{gut}^L
+ve	+ve	-ve	κ_{gut}^R	\dots	+ve	-ve	κ_{gut}^R
-ve	-ve	\dots	$\kappa_{\gamma ut}^L$	-ve	\dots	-ve	$\kappa_{\gamma ut}^L$
\dots	+ve	\dots	$\kappa_{\gamma ut}^R$	-ve	+ve	-ve	$\kappa_{\gamma ut}^R$

TABLE XI. Qualitative properties of the top polarization asymmetries and the forward-backward asymmetry of the scattered electron, allowing one to distinguish the effects.

scattered electron does not help. However, between A_x and A_z partial discrimination is achievable. In all cases A_x is negative and A_z is positive. However, absence of A_z and large negative A_x indicates the presence of $\kappa_{\gamma ut}^L$ in an unambiguous manner. Switching this, that is, when large A_z is present in the absence of A_x , indicates κ_{gut}^R . Qualitatively, κ_{gut}^L and $\kappa_{\gamma ut}^R$ shows similar behaviour, although there are some quantitative distinctions.

V. SUMMARY AND CONCLUSION

The possibility of measurable FCNC connected to top quark will clearly indicate dynamics beyond that of the Standard Model (SM). While the SM predicts very tiny effects arising through higher order quantum corrections, many popular extensions of the SM indicate possibility of much larger value for these couplings, close to what could be explored at LHC and other future colliders. The LHC in its high luminosity version could probe these couplings through searches of rare decays and single production of top quark. Being a top factory with very large statistics, the sensitivity of HL-LHC is quite competitive compared to any other planned future collider. However, when it comes to disentangling the effects of many possible couplings (like $tq\gamma$, tqZ , tqg), colliders with electronic initial states stand with clear advantages. In this work we have demonstrated the uniqueness of high energy electron-proton collider in this respect.

The process studied, namely the production of single top quark in association with a light jet and scattered electron in electron-proton collisions ($e^-p \rightarrow e^-tj$) in the planned high energy facility of FCC-he, has the potential to fingerprint the presence of top quark FCNC involving photon and gluons. We have demonstrated the sensitivity of the collider with electron beam of 60 GeV and proton beam of 50 TeV, along with the possibility of electron beam polarization is not only detecting these FCNC, but in distinguishing the effects of different types of couplings. We have considered the leptonic decay of the top quark in our study. A way to fully reconstruct the top quark, even with a missing neutrino as presented in section IV is made use of in reconstructing the events. The process has no SM background with the same parton level final state. However all possible

processes that could mimic the final state at the detector are considered in the study. MonteCarlo event generator, MadGraph5 is used to generated the signal and background events. With the help of Delphes package using a re-tuned detector card, effects of detector on the particle identification and energy and momentum measurements are incorporated. MadAnalysis is used to analyse the events and for final selection enhancing signal over background, with the help of appropriate kinematic regions. We could contain the background events to the level of a few tens at the expected luminosity of 2 ab^{-1} . With such reduced background, we have demonstrated that the presence of couplings to the level of a few times 10^{-2} TeV^{-1} can be probed at this collider with the process considered. This corresponds to the branching fractions of $BR(t \rightarrow u\gamma) \leq 4 - 7 \times 10^{-6}$ and $BR(t \rightarrow c\gamma) \leq 1 - 2 \times 10^{-5}$, depending on if the coupling is right-handed or left-handed. The corresponding limits on the gluon couplings lead to $BR(t \rightarrow u g) \leq 1.7 \times 10^{-6}$ and $BR(t \rightarrow c g) \leq 3 - 4 \times 10^{-5}$. Further, effective use of top quark polarization asymmetries, forward-backward asymmetry of the scattered electron, along with the effect of electron beam polarization on the cross section, it is possible to fully disentangle the effects of the four relevant couplings considered in the study.

ACKNOWLEDGMENTS

We acknowledge fruitful discussions within the Higgs and top physics study for LHeC and FCC-he group in customising the detector card used in this analysis. SB and PP thank the DST-FIST grant SR/FST/PSII-020/2009 for offering the computing resources needed by this work. PP is thankful to Department of Physics, Concordian University, for their hospitality during the manuscript preparation of this work.

-
- [1] S. L. Glashow, J. Iliopoulos, and L. Maiani, *Meeting of the Italian School of Physics and Weak Interactions Bologna, Italy, April 26-28, 1984*, Phys. Rev. **D2**, 1285 (1970).
 - [2] J. A. Aguilar-Saavedra, *Particle physics phenomenology at high energy colliders. Proceedings, Final meeting of the European Union Network, Montpellier, France, September 26-27, 2004*, Acta Phys. Polon. **B35**, 2695 (2004), arXiv:hep-ph/0409342 [hep-ph].
 - [3] G. Aad *et al.* (ATLAS), Phys. Lett. B **800**, 135082 (2020), arXiv:1908.08461 [hep-ex].
 - [4] V. Khachatryan *et al.* (CMS), JHEP **04**, 035 (2016), arXiv:1511.03951 [hep-ex].
 - [5] G. Aad *et al.* (ATLAS), Eur. Phys. J. **C76**, 55 (2016), arXiv:1509.00294 [hep-ex].
 - [6] V. Khachatryan *et al.* (CMS), JHEP **02**, 028 (2017), arXiv:1610.03545 [hep-ex].
 - [7] M. Aaboud *et al.* (ATLAS), JHEP **07**, 176 (2018), arXiv:1803.09923 [hep-ex].
 - [8] (2019).
 - [9] A. M. Sirunyan *et al.* (CMS), JHEP **06**, 102 (2018), arXiv:1712.02399 [hep-ex].
 - [10] M. Aaboud *et al.* (ATLAS), JHEP **10**, 129 (2017), arXiv:1707.01404 [hep-ex].
 - [11] ATLAS Collaboration (ATLAS Collaboration), *Expected sensitivity of ATLAS to FCNC top quark decays $t \rightarrow Zu$ and $t \rightarrow Hq$ at the High Luminosity LHC*, Tech. Rep. ATL-PHYS-PUB-2016-019 (CERN, Geneva, 2016).
 - [12] A. Papaefstathiou and G. Tetlalmatzi-Xolocotzi, Eur. Phys. J. C **78**, 214 (2018), arXiv:1712.06332 [hep-ph].
 - [13] Q.-H. Cao, S.-L. Chen, Y. Liu, and X.-P. Wang, Phys. Rev. **D100**, 055035 (2019), arXiv:1901.04643 [hep-ph].
 - [14] H. Khanpour, (2019), arXiv:1909.03998 [hep-ph].
 - [15] K. Oyulmaz, A. Senol, H. Denizli, A. Yilmaz, I. Turk Cakir, and O. Cakir, Eur. Phys. J. C **79**, 83 (2019), arXiv:1811.01074 [hep-ph].
 - [16] O. Cakir, A. Yilmaz, I. Turk Cakir, A. Senol, and H. Denizli, (2018), arXiv:1809.01923 [hep-ph].

- [17] S. Behera, R. Islam, M. Kumar, P. Poullose, and R. Rahman, (2018), arXiv:1811.04681 [hep-ph].
- [18] W. Liu and H. Sun, Phys. Rev. **D100**, 015011 (2019), arXiv:1906.04884 [hep-ph].
- [19] E. Alici and M. Kksal, (2019), arXiv:1905.00588 [hep-ph].
- [20] K. Y. Oyulmaz, A. Senol, H. Denizli, and O. Cakir, Phys. Rev. **D99**, 115023 (2019), arXiv:1902.03037 [hep-ph].
- [21] H. Khanpour, S. Khatibi, M. Khatiri Yanehsari, and M. Mohammadi Najafabadi, (2014), arXiv:1408.2090 [hep-ph].
- [22] J. A. Aguilar-Saavedra, Nucl. Phys. **B812**, 181 (2009), arXiv:0811.3842 [hep-ph].
- [23] J. Alwall, R. Frederix, S. Frixione, V. Hirschi, F. Maltoni, O. Mattelaer, H. S. Shao, T. Stelzer, P. Torrielli, and M. Zaro, JHEP **07**, 079 (2014), arXiv:1405.0301 [hep-ph].
- [24] T. Sjostrand, S. Mrenna, and P. Z. Skands, JHEP **05**, 026 (2006), arXiv:hep-ph/0603175 [hep-ph].
- [25] M. Cacciari, G. P. Salam, and G. Soyez, Eur. Phys. J. **C72**, 1896 (2012), arXiv:1111.6097 [hep-ph].
- [26] J. de Favereau, C. Delaere, P. Demin, A. Giammanco, V. Lematre, A. Mertens, and M. Selvaggi (DELPHES 3), JHEP **02**, 057 (2014), arXiv:1307.6346 [hep-ex].
- [27] E. Conte, B. Fuks, and G. Serret, Comput. Phys. Commun. **184**, 222 (2013), arXiv:1206.1599 [hep-ph].
- [28] I. Antcheva *et al.*, Comput. Phys. Commun. **180**, 2499 (2009), arXiv:1508.07749 [physics.data-an].
- [29] F. Boudjema and R. K. Singh, JHEP **07**, 028 (2009), arXiv:0903.4705 [hep-ph].
- [30] R. M. Godbole, S. D. Rindani, and R. K. Singh, JHEP **12**, 021 (2006), arXiv:hep-ph/0605100 [hep-ph].